Direct stochastic simulation of Ca²⁺ motion in *Xenopus* eggs

Y.-B. Yi,[1] H. Wang,[1] A. M. Sastry,[1,2,*] and C. M. Lastoskie[2,3]

[1]*Department of Mechanical Engineering, University of Michigan, Ann Arbor, Michigan 48109, USA*

[2]*Department of Biomedical Engineering, University of Michigan, Ann Arbor, Michigan 48109, USA*

[3]*Department of Civil and Environmental Engineering, University of Michigan, Ann Arbor, Michigan 48109, USA*

(Received 4 February 2005; published 29 August 2005)

The release of important intracellular ions has been widely modeled using two approaches, namely, (1) Fickian diffusion, in which sometimes tensorial diffusion coefficients are used to fit observed temporally varying concentrations of calcium, and (2) cellular automata, which produce a set of localized finite difference equations that result in complex global behavior. Here, we take a different approach, employing some assumed, *a priori*, distribution of ion-binding proteins in the cell, and some assumed biochemical capture and release characteristics to explain ionic motion, and ultimately, distribution. We study several scenarios for ion distribution, based on differences in binder action and distribution. The numbers and strengths of ion binders, spatial variation in inositol 1,4,5-triphosphate concentration, together with the escalating distribution of ionic diffusion speed, are found to be key factors leading to concavity in the Ca²⁺ wave shape. We also offer an explanation for geometrical effects on previously observed ion diffusion speeds in the cellular cortex of the *Xenopus laevis* egg during fertilization, based on an angle-of-view correction.

PACS number(s): 87.14.−g

I. INTRODUCTION

Cascades, waves, "bursts," "blips," and "puffs" of ionic calcium are associated with intracellular phenomena spanning fertilization, cell growth, muscle contraction, liver metabolism, and gene transcription [1]. Extracellular fluxes of ionic calcium are associated with wound healing and insulin secretion, among other physiological functions [2]. But these types of intra- and extracellular calcium transport has so far defied unified characterization, precisely because of the multifarious roles of calcium in signaling, and the widely varying magnitudes of fluxes associated with each role (Table I) [3–7].

Bootman *et al.* [8] and Callamaras *et al.* [9] were among the first workers to characterize intracellular Ca²⁺ signaling phenomena as hierarchical events. By histamine-stimulated generation of inositol triphosphate (IP₃) in Hela cells, Bootman *et al.* [10] identified three levels of calcium signaling: " Ca²⁺ blips" from single IP₃ receptors (IP₃R), intermediate " Ca²⁺ puffs" emanating from clusters of IP₃R, and global Ca²⁺ waves. As later enunciated by Blaustein and Golovina [11], emerging structural information about endoplasmic reticulum (ER) Ca²⁺ store organization is required to deconvolve the sources, behaviors, and significance of a variety of local and global Ca²⁺ signals in the nervous system. In particular, the endoplasmic reticulum (ER) Ca²⁺ stores in neurons consist of spatially distinct compartments that are individually loaded and unloaded.

Transitions among levels of Ca²⁺ release are putatively accomplished by coordination among IP₃, IP₃R, and Ca²⁺ concentrations. Release of calcium stores from the endoplasmic reticulum is cooperatively activated by binding of inositol (1,4,5)-triphosphate and Ca²⁺ on the inositol (1,4,5)-

triphosphate receptor [12]. Bootman *et al.* [13] verified experimentally the large number of Ca²⁺ stores within a cell. The binding of a calcium ion to the site exposed by IP₃ ligation activates the IP₃R channel, releasing calcium stores from the ER [14]. Calcium discharge into the cytosol is self-inhibited [15] by the binding of another Ca²⁺ to a second site in the IP₃R binding core. Ca²⁺ binding at this site putatively induces another conformational change which closes the channel, thus safeguarding against potentially explosive feedback from spontaneous channel opening [12]. Although the transduction mechanism for gate closure is not yet understood, the presence of a second, inhibitory Ca²⁺ binding site on IP₃R is supported by the bell-shaped dependence of IP₃R channel current on the free cytosolic Ca²⁺ concentration [14]. Propagation of the trigger-diffusion-trigger process by the IP₃ and Ca²⁺ coagonists ultimately forms a self-limiting, fertilization-induced Ca²⁺ "wave." Capacitive entry of extracellular calcium may be further instigated at this point by complexation of an IP₃R with a depleted lumenal store with the triphosphate subunit of the Ca²⁺ channel in the plasma membrane [16].

In this paper, we present a stochastic model for the IP₃R-activated intracellular Ca²⁺ transport. We focus on this transport pathway in recognition of its established importance as the principal mechanism for initiation and propagation of intracellular Ca²⁺ waves and for influx of extracellular Ca²⁺. The spatial distribution of the channel-activating coagonist IP₃ thus is an important consideration in the development of the model presented herein.

A. Modeling of calcium motion: Previous work

In many Ca²⁺ wave phenomena, e.g., fertilization [17], Ca²⁺ is thought to diffuse relatively slowly, across relatively large intracellular spaces, and thus follow the formalisms of diffusion theory. Analytical and numerical formulations have

*Corresponding author. Electronic address: amsastry@umich.edu

TABLE I. A chronological list of some reported experimental findings, related to calcium release events.

Authors	Year	Cell type	Phenomenon	Amplitude (nM)	Diameter (μm)	Peak duration (s)	Method
Deguchi and Osanai	1994	Oocytes of marine bivalves	Ca^{2+} wave	N/A	100	20	Sperm induced
Horne and Meyer	1997	RBL (rat basophilic leukemia) cell	Ca^{2+} blips	50 ± 10	<2	<0.033	IP_s induced
Bootman *et al.*	1997	HeLa cell	Ca^{2+} blips	<40	N/A	N/A	Histamine stimulated
Bootman *et al.*	1997	HeLa cell	Ca^{2+} puffs	>50	$2.5 \sim 5$	$3 \sim 10$	Histamine stimulated
Callamaras *et al.*	1998	*Xenopus* oocytes	Ca^{2+} puffs	N/A	3.0	$0.2 \sim 0.5$	IP_s induced
Fontanilla and Nuccitelli	1998	*Xenopus* oocytes	Ca^{2+} wave	700	1200	<30	Sperm induced
McDougall *et al.*	2000	Sea urchin eggs	Ca^{2+} wave	N/A	80	20	Sperm induced
Tovey *et al.*	2001	HeLa cell	Ca^{2+} puffs	127 ± 143	3.7 ± 0.6	<10	Histamine stimulated
Tovey *et al.*	2001	16HBE14o cell	Ca^{2+} puffs	178 ± 108	3.2 ± 0.8	<20	ATP stimulated
Tovey *et al.*	2001	SH-SY5Y cell	Ca^{2+} puffs	123 ± 105	3.0 ± 0.6	$5 \sim 10$	Carbachol stimulated
Marchant *et al.*	2001	*Xenopus* oocytes	Ca^{2+} puffs	N/A	2.5	$18 \sim 100$	IP_s induced

been developed for diffusion problems in both homogeneous and heterogeneous domains [18], and software packages are presently available to solve the diffusion equation within biological cells [19,20]. There is an attendant body of literature on the well-posedness of field solutions in the presence of jumps or discontinuities in concentrations of an ionic species over a membrane [21]. It is important to note that the Brownian motion assumed to produce diffusive mass transfer does not result in a particle velocity. By definition, the diffusion coefficient is

$$D = \frac{\delta^2}{2\tau},\tag{1}$$

where δ is the distance that the particle travels in the characteristic time period τ. Thus, the actual particle speed results in a displacement proportional to the square root of time in ordinary diffusion. Nevertheless, a "diffusion speed" can still be defined as the distance between two adjacent points in the direction of wave propagation, divided by the time taken by the wave front of a certain amplitude to traverse that distance. This definition of diffusion speed is used throughout the current paper.

A comprehensive review of various mathematical models for both intra- and intercellular Ca^{2+} diffusion was conducted recently [22]. Most of the models surveyed assumed reaction-diffusion processes for dispersion of Ca^{2+}, and assumed initial, spatial distributions of Ca^{2+} stores, either as continuum distribution functions, or as discrete, stochastically distributed release sites [23,24]. However, these models typically ignore the structural features of the cell, including ER distribution and organelle location. Bar *et al.* [25], for example, developed a set of probabilities for the opening and closing of calcium channels, which were assumed dependent upon calcium concentration. Falcke *et al.* [26], using a lattice of stochastic channel clusters, demonstrated a clear transition from isolated release events to steadily propagating waves, with increasing IP_3 concentration. Gil *et al.* [27] used a random walk model to simulate discrete three-dimensional (3D) diffusion, and kinetic reactions of ions and buffers. However,

none of these models assumed both a full-size three-dimensional cell boundary and realistic parameters pertaining to the ion and protein binder concentrations. In the study by Gil *et al.* [27], for example, the numerical model was restricted to a conical subdomain of the whole cell.

Several successful models have been developed to model motion of global calcium waves. Of particular interest in the present work are the coupled experiments and simulations of Wagner *et al.* [28], who used *Xenopus laevis* eggs to validate their continuum diffusion model. They established that inhomogeneous calcium release near the plasma membrane is required to explain the temporal and spatial dependencies of the shape and speed of Ca^{2+} waves.

B. Fertilization-induced Ca^{2+} waves in *Xenopus* eggs

The spherical *Xenopus laevis* oocyte is a well-studied model cell for study of fertilization-induced calcium waves [17] due in part to its relatively large size (>1 mm [29]). At the sperm entry site on the egg surface, a Ca^{2+} wave initiates and propagates across the egg until reaching the antipode, i.e., the surface location opposite to the sperm entry point. Callamaras *et al.* [9] investigated the activation of elementary calcium release events and their coordination to generate Ca^{2+} waves in *Xenopus* oocytes, by controlling the concentration of IP_3 through photorelease of IP_3 from a caged precursor. They found that the initiation of calcium liberation depended upon IP_3 concentration, but the subsequent regenerative increase in Ca^{2+} flux depended upon local calcium feedback, and was largely independent of IP_3 concentration. Fontanilla and Nuccitelli[17] carried out perhaps the most exhaustive study of this phenomenon, by imaging the fertilization-induced calcium wave in a 1.2 mm *Xenopus* oocyte via confocal microscopy. The ratiometric fluorescent dyes were used to correct for the differential attenuation artifact of the fluorescence signal resulting from the spherical shape of the egg. They found that (1) the wave traverses the entire egg, converges uniformly on the antipode, and remains concave through its entire motion; (2) the wave velocity through the center is slower than that in the cortex; (3) the

cortical wave velocity is minimum at center and maximum at the beginning and end.

Wagner *et al.* [28] attempted to rationalize these results using a diffusion model implemented in a combined finite element–finite difference model, i.e., a formulation of the finite element method was applied in the 2D circular domain, using linear basis functions and triangular elements. They suggested that the inhomogeneous distribution of IP$_3$ along the cortex produced varying speeds of calcium ions, resulting in a concave wave. Further, in Bugrim and Wagner's recent work [30,31], it was revealed that the fertilization-induced Ca²⁺ wave is always accompanied by a wave of IP$_3$ production, and that IP$_3$, rather than Ca²⁺, is more likely to be responsible for triggering the Ca²⁺ wave in *Xenopus* eggs. Further, in several published models [28,32], the termination of ion release from stores has been controlled by increase in IP$_3$ concentration. Bootman and Lipp [33], for example, assumed the cytosolic Ca²⁺ concentration to relate to IP$_3$ receptor activation, following a bell-shaped curve.

By contrast, we herein develop a direct, stochastic simulation methodology for Ca²⁺ motion, which reflects the discreteness of release events, and can include a variety of complex mechanisms of Ca²⁺ release and uptake in spherical *Xenopus* eggs. Indeed, our relatively recent ability to directly image intracellular structures and release sites [34,35] motivates us to consider models that allow direct incorporation of detailed information about membrane structures, rather than provide a backfit of observed diffusion waves using a small number of coefficients. Our objectives in the present paper are thus fourfold. We wish to

(1) reconstruct the 3D diffusion model for a *Xenopus* egg, and reconsider the findings of previous workers [17,28] using a model corrected for viewing angle of the experiment;

(2) demonstrate the limitations of a diffusion model as applied to the sperm-induced calcium wave shape in a *Xenopus* egg, and to demarcate the limited types of wave shapes attainable via alteration of local diffusion coefficients only;

(3) demonstrate the ability of a stochastic model to capture the sperm-induced calcium wave shape in a *Xenopus* egg, assuming varying concentrations of calcium stores near the membrane; and

(4) provide a minimum set of simulable parameters, obtainable from biochemical experiments, to inform similar models for generalized intracellular ion transport.

Binders in these direct simulations are assumed to respond to "triggers" for calcium release. Calcium ions captured on the most readily exchangeable low-affinity actin binding sites could be represented using an effective capture radius derived from the orientation-averaged potential. Recently, for example, we have calculated the binding energy exerted by the actin molecule on a free calcium ion when the high- and medium-affinity calcium binding sites on actin are already occupied by calcium ions [36]. Actin has one tightly binding site of nanomolar affinity for calcium [37], four additional medium-affinity calcium sites with equilibrium constants in the 0.1 m*M* range [38], and five weakly binding sites with calcium affinities on the order of 10 m*M* [39].
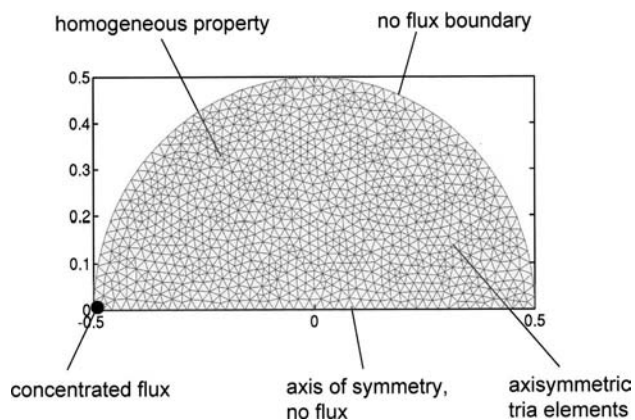

FIG. 1. An axisymmetric continuum diffusion model. The pulse duration is 0.01 s; total simulation time is 1 s.

II. METHODS

A. Numerical implementation of a simple, 3D diffusion model with an angle-of-view correction for interpretation of experiments

Fick's equation can be derived via a random walk model, or using a control volume analysis on mass flow induced by a spatial gradient in concentration, and can be written

$$D \nabla \cdot (\nabla u) = \frac{\partial u}{\partial t}, \tag{2}$$

where u is the concentration of Ca²⁺, D is a diffusion coefficient, and t is time. In an infinite, three-dimensional, homogeneous space, Ca²⁺ concentration due to a short pulse would be a three-dimensional Gaussian distribution function of Ca²⁺ concentration u with respect to the distance r. Thus, in a homogeneous domain without boundary constraints, the wave front maintains a convex, spherical shape. However, in a homogeneous circular or spherical domain, this wave is inherently concave. This can be demonstrated by assuming a point pulse source of calcium within a spherical geometry, and no influx at the boundary. If the initial concentrated source is applied on $r=R$, $\theta=\pi/2$ at $t=0$, the resulting profile of concentration distribution $u(r,\theta,t)$, is independent of ϕ, and thus Eq. (2) can be simplified as

$$\frac{\partial u}{\partial t} = D\left(\frac{\partial^2 u}{\partial r^2} + \frac{2}{r}\frac{\partial u}{\partial r} + \frac{1}{r^2}\frac{\partial^2 u}{\partial \theta^2} + \frac{\cot\theta}{r^2}\frac{\partial u}{\partial \theta}\right). \tag{3}$$

Analytic solutions of the above equation via Legendre polynomials are available for some simplified problems, with homogeneous boundary conditions. An explicit, analytic solution for the current problem is not readily available, if at all, in the present problem due to the inhomogeneity of the boundary conditions. Thus, we proceed with numerical solution of Eq. (3). We assume no flux at the boundaries, i.e., no intercellular Ca²⁺ can enter the cell through the membrane, per

$$\nabla u = \mathbf{0}|_{r=R}. \tag{4}$$

Shown in Fig. 1 is the axisymmetric, continuum finite element model used to determine the three-dimensional Ca²⁺
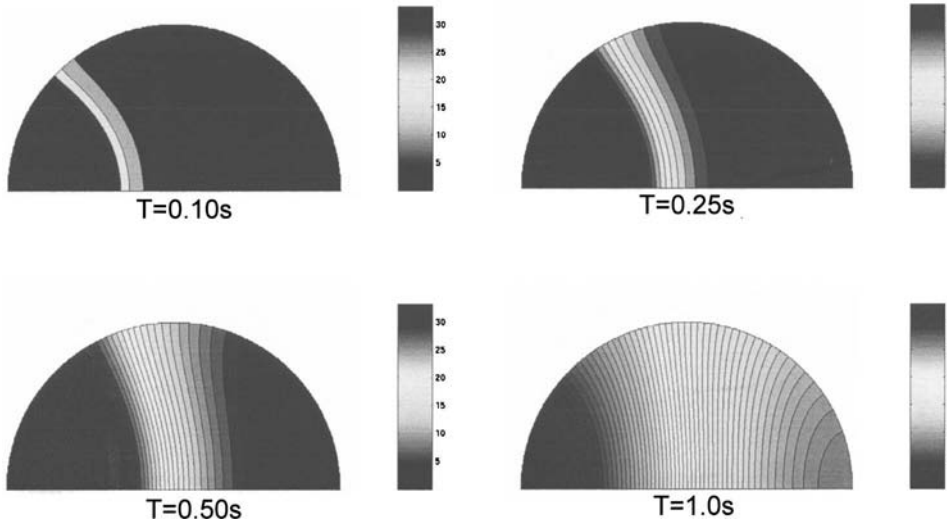
FIG. 2. Simulation result for an axisymmetric continuum model, showing the wave-front shape change from convex to concave.

distribution in spherical *Xenopus* eggs undergoing fertilization. The numerical solution is shown in Fig. 2, with conditions described above.

Confocal microscopy allows three-dimensional visualization of wave-front progression by assembly of two-dimensional image slices [40]. However, misalignment of the slices with respect to the direction of wave propagation biases calculation of the wave-front velocity. The proper plane to measure wave speed is the plane anchored by the sperm entry site and defined by the angle of inclination of the sperm relative to the egg, i.e., the place *OAGEF* in Fig. 3, assuming that the wave propagation is by definition normal to the egg membrane. The diffusion speed measured in the plane of the confocal microscope *OBDCH* is based on the arclength *BH*. If we assume constant angular diffusion speed ω in plane

FIG. 3. Effect of view angle on the observed ion diffusion speed.

OACEF, the length of arc *AF* is φR, in which R is the radius of the sphere; φ is the angle. The length of arc *BH* can be obtained as

$$\overline{BH} = R \cos^{-1}\left(\frac{\cos \varphi}{\cos \alpha}\right), \tag{5}$$

where α is the angle between the observation plane and the plane on which the diffusion actually takes place. The observed angular velocity of diffusion ω^* can be obtained via

$$\omega^* = \frac{d(\overline{BH}/R)}{dt} = \frac{d\left[\cos^{-1}\left(\dfrac{\cos \varphi}{\cos \alpha}\right)\right]}{dt} = \frac{\omega \sin \varphi}{\sqrt{\cos^2 \alpha - \cos^2 \varphi}}. \tag{6}$$

Subsequent interpretation of experimental data will employ this correction.

B. Direct simulation of dynamic ion exchange among binders

We denote the free ion concentration as ρ_i, the binder concentration as ρ_b, and the free ion speed as v. We further denote the maximum number of ions that a binder can contain as m, and the binder effective radius as a. The number of ions stored inside binders has a mean density $m\rho_b/2$. Conservation of ions requires

$$\frac{m\rho_b}{2} + \rho_i = m\rho_b, \tag{7}$$

which immediately yields a relation between ion and binder concentrations, as

$$\frac{\rho_i}{\rho_b} = \frac{m}{2}. \tag{8}$$

Clearly, there is a discrepancy between our understanding of the exchange as a dynamic process, and our characterization of a binding strength as an affinity, or molarity. But a relation can be derived between the equilibrium dissociation constant K_d and the statistical parameters used in this study, as follows.
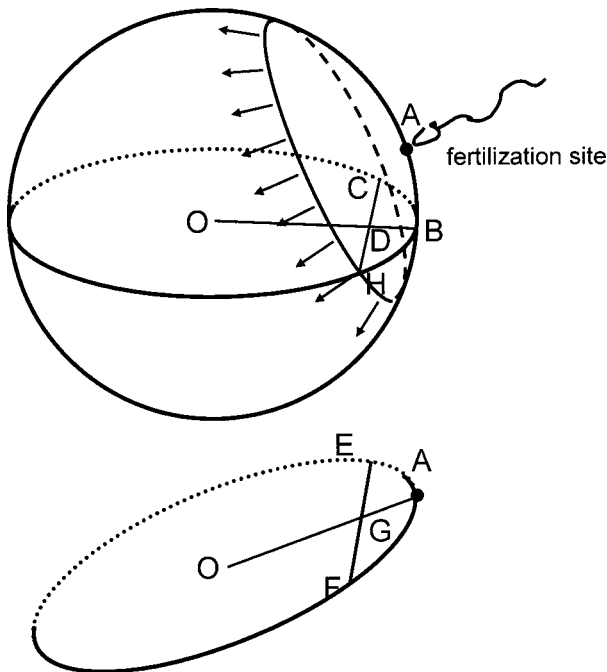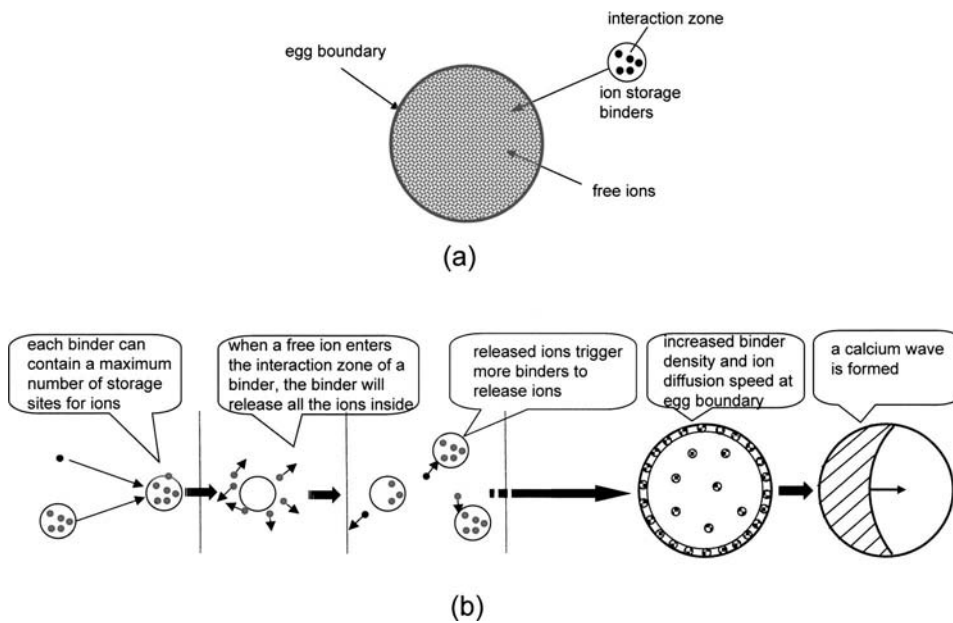
FIG. 4. Schematic of the stochastic simulation model for Ca^{2+} motion in *Xenopus* eggs: (a) ion binders can store and release ions; (b) the regenerative process of ion release forms the propagation of a calcium wave.

The equilibrium dissociation constant K_d is, by definition,

$$K_d = \frac{[A] \times [B]}{[AB]}, \tag{9}$$

where $[A]$ is the concentration of the free ions, Ca^{2+}, and $[B]$ is the binding site concentration for our present problem.

For the purpose of correlating the parameters obtained from a dynamic exchange simulation with the parameter K_d used to represent the equilibrium constant, we consider the dynamic equilibrium between the ions and binders and obtain $[A]=\rho_i$, $[B]=\rho_b/(m+1)$; $[AB]=\rho_b m/(m+1)$. Substituting these relations into the definition of K_d, we have immediately

$$m = \frac{\rho_i}{K_d}. \tag{10}$$

In the present model, the mean time elapsed between individual ion releases and captures is denoted the "binding time" T. T is a function of binder concentration ρ_b, binder effective radius a, and free ion speed v, per

$$T = \frac{1}{\rho_b a v}. \tag{11}$$

Therefore the binding time here is not a preset parameter; rather, it is determined by other parameters.

The behavior of each of the species in our simulations is described as follows. Each binder is assumed to contain a maximum number of binding, or storage, sites for ions (here, a maximum of five). An interaction zone around each binder is prescribed; the size of the interaction zone reflects the strength of binders, as schematized in Fig. 4. For simplicity, we use a circular or spherical domain centered on the binder to model this zone. No inertial effects, e.g., acceleration of ion or change in direction of motion, are considered in modeling an ion while it is entering the binding zone.

Two triggering mechanisms for release of ions are implemented, as simplified versions of the protein conformational changes known to occur in the presence of a change to the electromotive force field around an ion-binding protein. First, release of ions by a binder is triggered by sufficiently close approach of another ion; once the triggering occurs, all ions are released simultaneously. Second, a fixed binding time is assigned to each binder, to reflect the statistically random conformational changes occurring in proteins and triggering release of ions, apart from triggering due to local changes in concentration of the ionic species of interest. The high affinity (nanomolar) cation binding site in the actin cleft, for example, is readily exchangeable, with association and dissociation rate constants of 2.1×10^7 M^{-1} s^{-1} and 0.014 s^{-1}, respectively, for calcium on the ATP-bound actin monomer, and corresponding association and dissociation rate constants of 2.3×10^5 M^{-1} s^{-1} and 0.0015 s^{-1} for magnesium binding on the same site [37]. For a low probability of triggering apart from the first mechanism, this time may be set to infinity. Once emptied of ions (by either mechanism), binders are immediately able to absorb new ones, setting up the dynamic equilibrium.

Local concentrations of binders are cell specific; spatial arrangements of Ca^{2+} binders play an important role in determining wave-front shape. In Callamaras *et al.*'s investigation [9] on elementary Ca^{2+} release events in *Xenopus* oocytes, a curve was given for the numbers of release sites responding as a function of $[\text{IP}_3]$, from which it can be seen that ultimate number of responding sites is approximately $0.34/\mu$m on average. According to Bootman *et al.*'s study [13], on the other hand, if uniform distribution of release sites is assumed, there would be approximately 300 Ca^{2+} puff sites along a straight line with a length of 1.2 mm (i.e., the egg diameter). Based on this estimation, there could be 70 000 sites in the cross sectional plane of the egg, and in a full 3D spherical domain, we estimate that as many as 1.41×10^7 calcium release sites are available; the average number of ions stored in a single site exceeds 6500.

TABLE II. Simulation parameters used in the present stochastic model (parameters are normalized to domain diameter in the 2D simulation.)

	Time step dt (s)	Domain diameter	Binder speed	Max. ion number	Number of binders	Speed of free ions	Simulation time (s)	Binder radius
2D	0.01	0.5	0	5	600	0.5	2.5	0.005
3D	0.01	1.2 mm	0	5	1.4×10^7	150 μm/s	2.5	1 μm

We begin with a set of two-dimensional problems, which can be readily extended to three dimensions. Other assumptions include homogeneous distribution of binders, concentrated distribution of stores in cortical region, and assigned diffusion speed versus simulated diffusion speed based on local concentration of Ca^{2+} ions. Considering the large number of sites as well as the large number of ions stored in each site, full-scale simulation is extremely computationally intensive in both two-dimensional and three-dimensional problems. Therefore, while using the discrete model in simulating the elementary events, some averaging is required to obtain parameters for binders, ions, and calcium stores, and other physical parameters.

1. Simple diffusion simulation with uniformly distributed binders

The main parameters used in the simulations are given in Table II. A two-dimensional circular domain was used to represent a *Xenopus* egg; the Ca^{2+} wave was triggered by a single free sperm introduced at a certain location on the domain surface. We assumed homogeneous distribution of ionic binders in motion at a constant speed, within the domain. The boundary was assumed to be fully elastic, namely, free ions were reflected back with the same absolute velocity upon collision with boundaries.

2. Diffusion simulation with increased distribution of binders near the boundary

As a first alternative to Wagner *et al.*'s continuum approach [28] with a graded distribution of diffusive properties within the plane of fertilization, we simulated discrete binder distributions with biased densities near the boundaries. Specifically, the concentration of binders was doubled in the outer layer relative to the inside, to study the change in the resulting distribution of ions due to change in binder distribution. The thickness of this layer was fixed as 1/10 of the egg radius. The speed of released ions (0.5/s, normalized to the domain diameter) was assigned as the same as those in the center of domain.

3. Diffusion simulation with increased assumed diffusion speed near the boundary

As a second alternative to the continuum diffusion model of Wagner *et al.* [28], a faster diffusion speed was assumed for ions near the boundary. This could result from either high localized production of IP_3 at the plasma membrane [28], or the faster transport afforded by the relatively denser cytoskeletal proteins transporting ions near the membrane. The density of actin filaments within most cells is greatest within the cell cortex at the cell periphery, directly beneath the plasma membrane [41]. We doubled the velocity of the released ions in the boundary layer, in order to study the trend of change in the resulting distribution of ions due to change in ion velocity. As before, the concentration of binders was assumed to be uniform elsewhere in the domain. Other parameters remain the same as those in the model possessing homogeneous properties.

4. Diffusion simulation with increased distribution of binders and assumed diffusion speed near the boundary

Combining the previous two approaches, we simultaneously doubled the binder concentration and the velocity of the released ions in the boundary layer to investigate their combined effects on the wave-front shape, etc. Other properties remained the same as the previous models.

5. Full-size simulation model

By indexing binder positions, we extended the previously described two-dimensional models to three dimensions. Binder positions were stored in computer memory, and were checked at each iteration in examination of binder-ion interactions. Typically, only a few seconds were required by a SUN Blade series workstation to run a full-size two-dimensional simulation with 70 000 binding sites. By comparison, approximately 10–20 h were required to run a full-size three-dimensional simulation (with $>1.0 \times 10^7$ binding sites).

Similar to conditions simulated in the 2D model, we examined six cases: (1) uniform distribution of binder concentration and ion release speed in the entire egg; (2) doubled binder concentration in the boundary layer with respect to the interior of the cell; (3) doubled ion release speed in the boundary layer with respect to the interior of the cell; (4) linearly increased binder concentration and ion release speed, along the radial direction with respect to the interior of the cell; (5) quadratically increased binder concentration and ion release speed along the radial direction with respect to the interior of cell; and (6) constant binder concentration and ion release speed uniform in the interior of the cell, but doubled values of both in the boundary layer. Numerical values of model parameters are summarized in Table II.

6. Incorporation of IP_3 effects in the simulation model

IP_3 and Ca^{2+} production at the point of fertilization is followed by the diffusion of both species into the cell interior [42–44]. IP_3, which has a diffusion coefficient of 280 μm^2/s
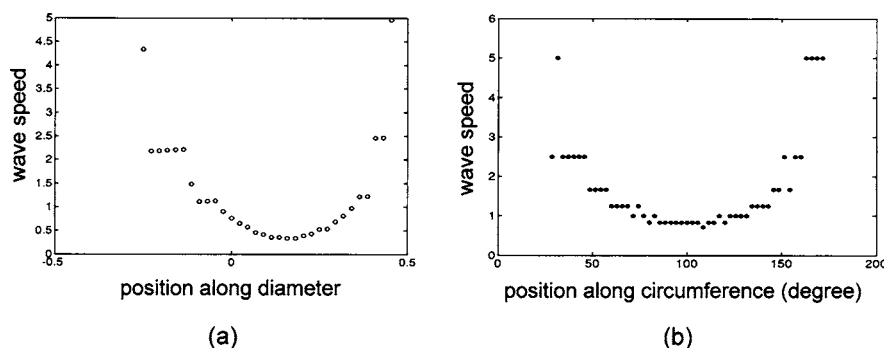
FIG. 5. Diffusion speed along the (a) diameter and (b) circumferential direction.

in the cytoplasm, propagates rapidly and serves as the global messenger, whereas Ca^{2+} with its smaller diffusion coefficient of 13 μm^2/s is less mobile and acts within restricted domains of ~5 μm within the cell [44]. Based on this signal transduction mechanism, Wagner *et al.* [28] hypothesized an exponential distribution of IP$_3$ concentration along both tangential and radial directions in the vicinity of the fertilization site. We incorporate this assumption into our simulation model to study the effect of varying concentration of IP$_3$ on the Ca^{2+} wave propagation. In this assumption, the radial distribution of IP$_3$ has the form

$$[\text{IP}_3] = I_s\{1 + I_h \exp[(r/r_c - 1)/I_w]\}, \qquad (12)$$

while the tangential distribution has the form

$$[\text{IP}_3] = I_h^* \exp[(r/r_c - 1)/I_w]\exp\{-[y/(I_w^* r_c)]^4\}, \qquad (13)$$

$$x < 333 \ \mu M,$$

where the constants involved are I_s=0.12 μM, I_h=1.0, I_h =0.84 μM, I_w=0.015, I_w^*=0.8; (x,y) is the Cartesian coordinate of a point in the egg with (0,0) at the center. Apparently the IP$_3$ concentration is maximal at the fertilization site and declines rapidly away from the site.

The relation between the concentrations of IP$_3$ and Ca^{2+} is complex [45–47]. Since it is not our intention to conduct a detailed study on IP$_3$ dynamics or feedback processes between IP$_3$ and Ca^{2+}, here we simply assume the relation is linear—that is, an increase of IP$_3$ concentration causes a proportional increase in the concentration of Ca^{2+}. The magnitude of the maximal increase of Ca^{2+} induced by IP$_3$ is normalized by the average concentration of cytosolic Ca^{2+}. Full 3D simulations are performed to investigate the effect of inhomogeneity of IP$_3$ concentration on the Ca^{2+} wave profile. To make the simulation tractable, here IP$_3$ concentration is considered as the only inhomogeneous property in the model while the ion speed and the binder distribution are assumed constant and uniform throughout. The radial and tangential gradients of IP$_3$ concentration are applied as sources of the initial triggering Ca^{2+} ions. These triggering ions are distributed tangentially and radially, depending on IP$_3$ distribution. Once the wave is triggered, localized Ca^{2+}-induced Ca^{2+} concentrations are superposed with the IP$_3$-induced Ca^{2+} increases. Since IP$_3$ concentration decays rapidly in the radial direction away from the fertilization size, the role of the tangential gradient of IP$_3$ dominates in the initial development of Ca^{2+} wave, which is consistent with the experiments in which a fast initial tangential wave propagation velocity was observed [17]. The simulation results are interpolated over a set of evenly spaced "grids" from which the cross sectional profile of the contour plots for the Ca^{2+} concentration distribution is generated.

III. RESULTS

We simulated the spatial and temporal changes in Ca^{2+} concentration during the wave propagation. Both the continuum diffusion model and stochastic model are used in the simulations for the purpose of comparison.

A. Reconsideration of the 3D continuum diffusion model

The numerical solution of the simple, 3D continuum diffusion model as discussed in the above section showed that the contour lines of Ca^{2+} concentration are concave near locations opposite to the source, i.e., after the wave front has traveled through the center. Similar phenomena were also observed under different loading or boundary conditions, implying the concave wave-front shape in the late stage of wave development is intrinsic to diffusion. In Figs. 5(a) and 5(b), we plotted the wave-front traveling speed versus locations on the diameter and circumference, respectively. The wave speed is greatest at the beginning and end, and is at a minimum at the center. This again agrees well with Fontanilla and Nuccitelli's experimental observation in which the cortical wave speed starts out rapidly, slows down as it approaches the center, and then speeds up again. However, this mechanism of geometrical shape alone is unable to explain why the wave-front shape turns to concave at the very beginning of the process, and why the wave speed is the fastest at the center on diameter. The introduction of nonuniformity in diffusion speed of the stochastic model (or, as a counterpart, nonuniform distribution of diffusivity in the continuous model) is thus a necessary assumption in successful explanation of the experimental observation. As we have seen, the measured diffusion speed ω^* is a function of viewing angle α, shown in Eq. (6) and in Fig. 6.

B. Direct simulations

The simulation results presented below follow the same sequence as in Sec. II. We begin with the simulation results from a simplified two-dimensional model; then the results
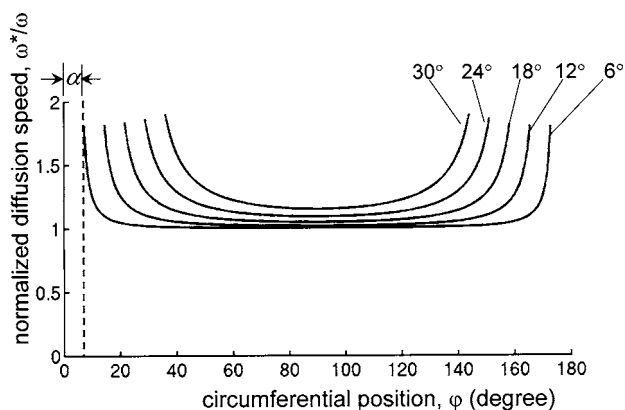
FIG. 6. Diffusion speed as a function of circumferential position under a different view angle.

from the full-size three-dimensional model with and without the explicit incorporation of IP$_3$ distribution.

In Fig. 7, the static images of wave propagation in homogeneous cytoplasm with uniformly distributed binders are sequentially presented at time interval of 0.5 s. In the images, each dot represents an individual ion. The wave initiates at a single point, at the fertilization site, then propagates to the antipode. Shown in Fig. 8 is a series of simulation frames for wave propagation resulting from doubling of the binder concentration in the boundary layer. In Fig. 9, the diffusion speed was doubled in the boundary layer, and thus the ions moved much faster in the outer part of the wave. Figure 10 shows the simulation results when both diffusion speed and binder concentration in the boundary layer were increased.

Examples of full-size simulations are shown in Fig. 11, where the ion concentration fields of wave propagation in the 3D full-size models are plotted. The diffusion speed and binder concentration are doubled in the thin outer layer. It should be pointed out that the quantity shown in the contour plot of Fig. 11 represents free ion concentration, rather than the individual ions previously presented in the plots of the reduced model. In addition, the discrete result data were interpolated over a "coarse mesh" to exhibit the dynamic, local variation of ion concentration. On the other hand, the 3D profile of the wave front in Fig. 11(a) was constructed by smoothing and interpolation of the ion concentration and
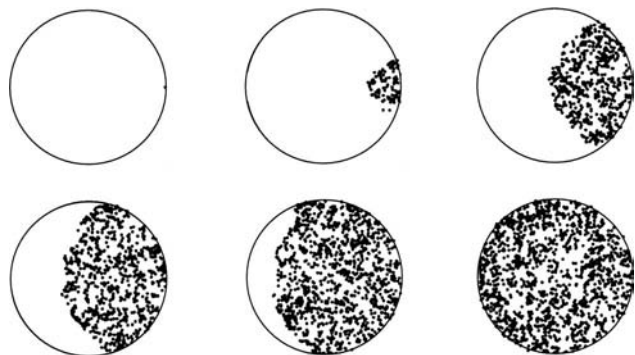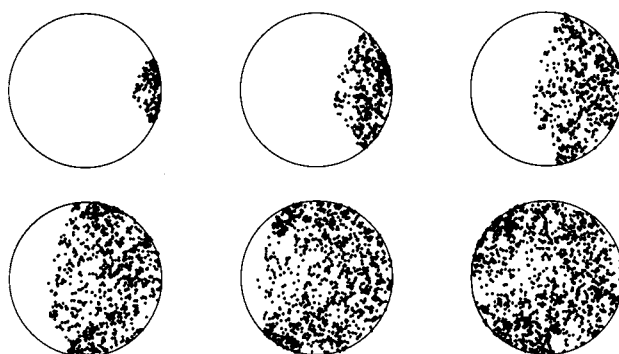

FIG. 8. Simulation of Ca^{2+} motion using the stochastic model. Binders doubled at the boundary layer.

then by mapping the isosurface of the resultant field. Figure 12 involves 1.4×10^7 binding sites and totally 7.0×10^7 ions.

The tangential gradient of IP$_3$, as given in Eq. (10), is presented in a plot against the angular position of the cortical location, as shown in Fig. 12. Nonuniformity in IP$_3$ concentration in the cortical region results in the tangential gradient of the initial Ca^{2+} distribution. This is equivalent to adding a thin layer of triggering Ca^{2+} to the system, which leads to the concavity in the Ca^{2+} wave fronts, as shown in the six consecutive images in Fig. 13. The simulation parameters used here are identical to those listed in Table II, except that the simulation time in this case is about 4.0 s, beginning with the image on the top left when the initial thin crescent of Ca^{2+} ions (induced by the cortical IP$_3$) start to initiate the wave, and ending with the image on the bottom right when the wave front reaches the antipode and the equilibrium is established. The time interval between two consecutive images in Fig. 13 is approximately 0.5 s, except for the last image where it takes a little longer (2 s) for the system to reach a dynamic equilibrium phase, since the wave front would bounce back after reaching the antipode.

IV. DISCUSSION

Our present approach differs from some continuum models in which depletion is not modeled. It should be pointed out that although our study is not focused on the biochemical processes underlying the different behaviors of Ca^{2+} chan-
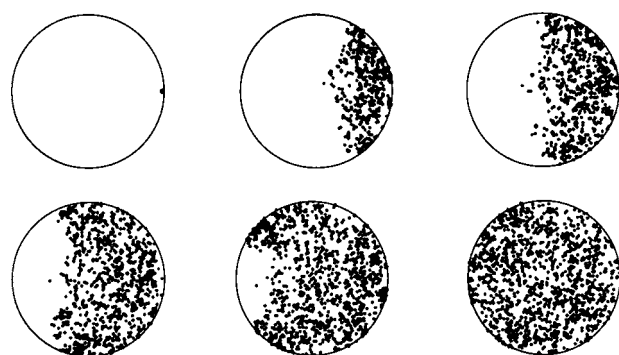

FIG. 7. Simulation of Ca^{2+} motion using the stochastic model. Homogeneous properties are assumed.

FIG. 9. Simulation of Ca^{2+} motion using the stochastic model; ion diffusion speed doubled at the boundary layer.
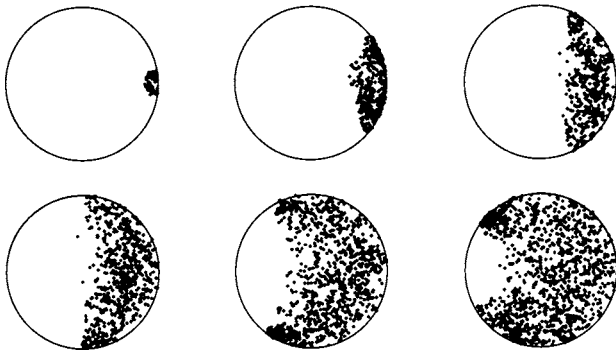
FIG. 10. Simulation of Ca²⁺ motion result using the stochastic model; both ion storage capacity and ion diffusion speed doubled at the boundary.

nels, these behaviors can actually be included in the model by simply setting up rules for ion release from binders. As discussed previously, modeling of calcium diffusion as a global phenomenon cannot explain some experimental observations. Almost all the existing models, including the cellular automata approach, ignore the structural complexity of cells and eggs. In contrast, we proposed a multiscale modeling scheme for the calcium diffusion problem. The local modeling is stochastic and can include different release mechanisms (e.g., calcium blips and puffs) and local structures (e.g., ER, mitochondria, and microtubules). Local spatial distribution of ion binders combined with mechanisms for release can produce special mechanisms of ion diffusion, e.g. anisotropic diffusion of calcium near the cortex. Specific findings from our simulations follow.

A. Reconsideration of the 3D continuum diffusion model

It has been seen from Figs. 5 and 6 that the wave speed is greatest at the beginning and end, and is at a minimum at the center. This agrees with experimental findings [17], in which the cortical wave is initially fast, but slows down as it approaches the center, and then speeds up again. However, this alone is unable to explain why the wave-front shape becomes concave at the very beginning of the process, and why the wave speed is the fastest at the center on diameter. The introduction of nonuniformity in diffusion speed of the stochastic model (or, as a counterpart, nonuniform distribution of diffusivity in the continuous model) is thus a necessary assumption in successful explanation of the experimental observation.

Per Fig. 6, the wave in the observation plane starts some time later than the wave as actually initiated. The time lag between the real and observation starting times is α/ω. The wave in the observation plane initially proceeds rapidly, but slows down and reaches a minimum value $1/\cos^2 \alpha$ as it passes through the center, whereupon it speeds up again. The phenomenon agrees with the cortical diffusion speed profile reported by the previous experiments [17]. It is also found that the measured diffusion speed ω^* is always greater than the actual diffusion speed ω for any α. In addition, the observed diffusion speed increases with an increase of α. This is even more apparent at locations away from the center.

In short, the variation in view angle can alter the diffusion speed. The fact that small changes in α could result in significant changes of the measured wave speed makes it extremely important in experiments to properly align the observation plane to the plane where the diffusion actually occurs. If the precise alignment cannot be realized in experiments,
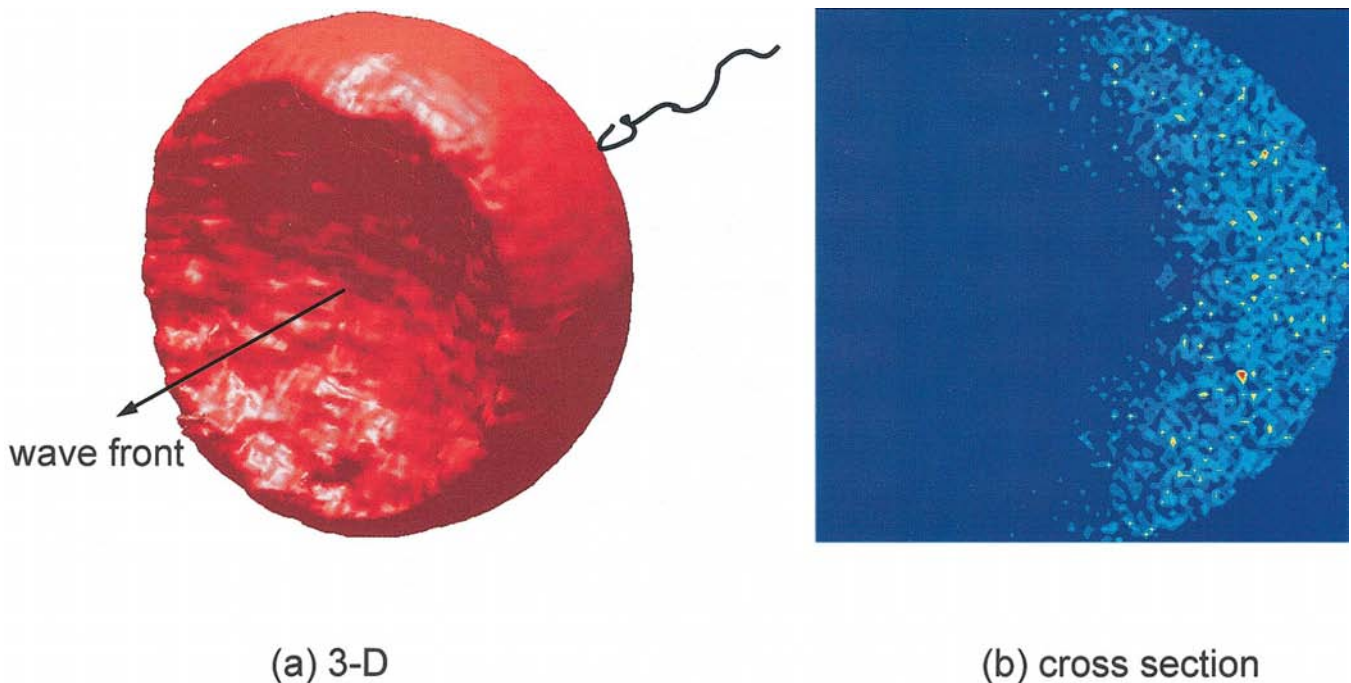

(a) 3-D

(b) cross section

FIG. 11. (Color) Ca²⁺ concentration in 3D (a) and its cross sectional plane (b) full-size stochastic models. Linear interpolation was used in production of the contour plots.
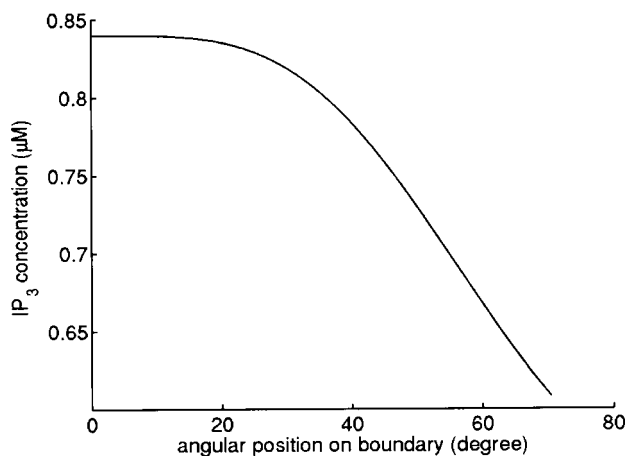
FIG. 12. Assumed distribution of IP$_3$ concentration as a function of angular position on the cortical surface. The center of the coordinate system is located at the center of the egg and zero degree of angle corresponds to the fertilization site.

the effect of view angle must be taken into consideration via Eq. (6) during the evaluation of the diffusion properties.

B. Direct simulations

In simple diffusion simulation with uniformly distributed binders as shown in Fig. 7, after 2.5 s, the entire domain is full of ions and reaches a status of dynamic equilibrium. Interestingly, according to Eq. (8), the number of free ions is approximately $0.5 \times 5 \times 600 = 1500$ at equilibrium. Since the process is stochastic, the wave front is not smooth, though it is approximately convex throughout the process, and circular at the boundary upon initiation, due to uniform distribution of binders, identical speed of released ions, and reflectivity of the boundary. This differs markedly from the result of the continuum model studied, in which a transition of the wave front shape is observed even if the homogeneous properties of cytoplasm are assumed.

The convex wave front resulting from diffusion simulations with increased distribution of binders near the boundary (as represented by Fig. 8) is materially similar to that resulting from a model having a uniform distribution of binders. However, as the wave propagates, the convex shape flat-
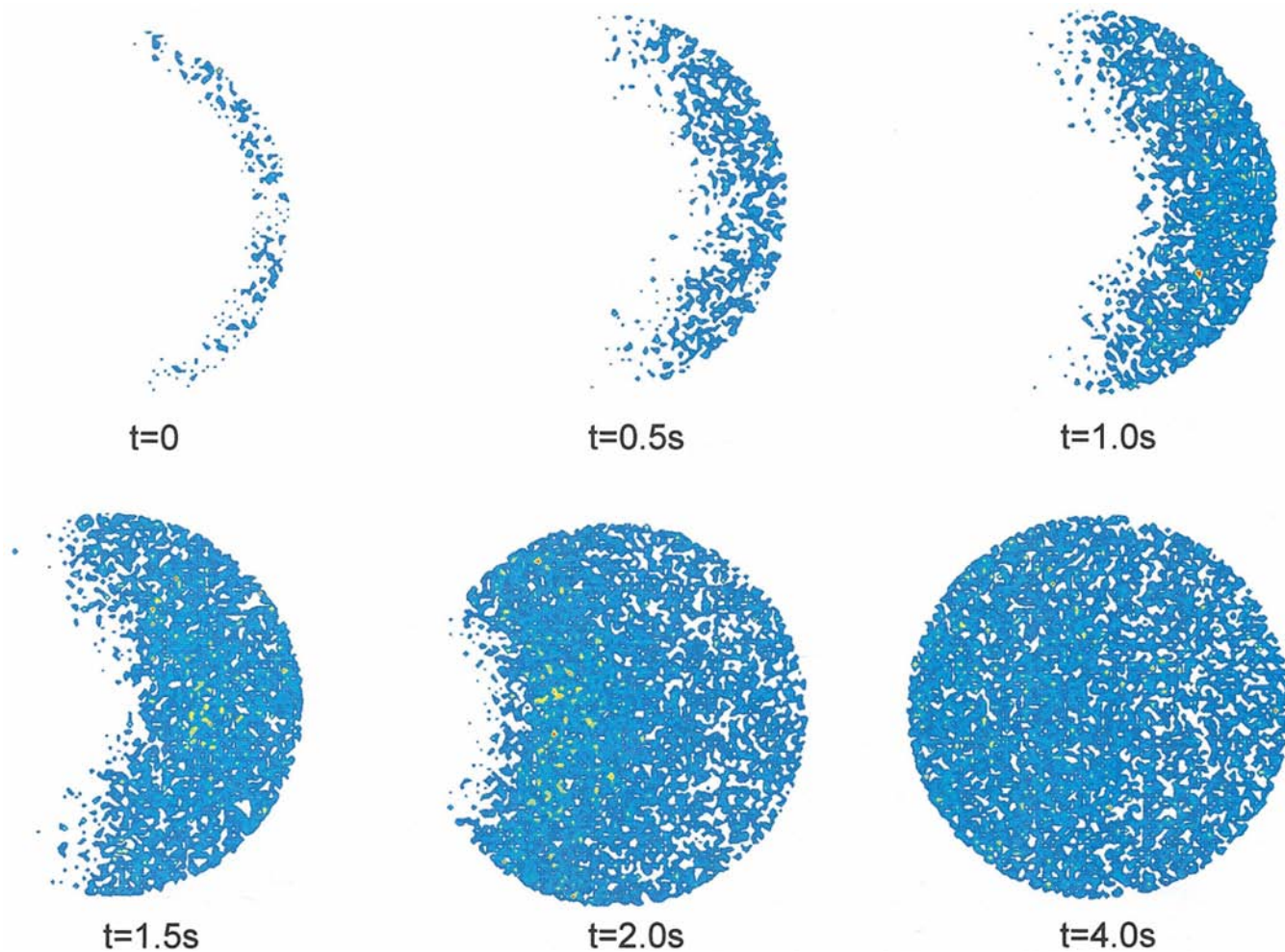

FIG. 13. (Color) Simulation result of Ca^{2+} motion using inhomogeneous IP$_3$ distribution. t represents simulation time. Contour plots on the cross sectional plane are shown. Local concentration of Ca^{2+} lower than 10% of the maximum value is shown empty in the plots.

tens in comparison with the former model. This results from the higher probability of triggering binders and hence the higher density of free ions in cortical regions. This higher probability increases wave speed in the tangential direction. Nevertheless, this increase of speed alone is not high enough to induce a concave wave front.

Doubling of diffusion speed in the boundary layer (Fig. 9) resulted in a sufficiently high increase in ion speed to induce a reversal in the wave front shape, from convex at the initiation site, to concave at the antipode. The transition occurred after the wave front reached the center of the egg. Apparently, the degree of concavity is determined by the speed of free ions at the boundary relative to those in the interior. Use of a continuous, linear or quadratic distribution profile in the radial direction also produced a similarly concave wave front.

Obviously, simultaneous increase in diffusion speed and binder concentration in the boundary layer encourages development of concavity in the wave relative to increasing either parameter singly, as shown by comparisons of Figs. 8–10.

Unsurprisingly, similar results were found in the full-scale simulation as shown in Fig. 11, in comparison to the reduced model: change of binder concentration distribution alone does not affect the wave-front shape significantly; a concave wave will not form unless the inhomogeneity of ion speed distribution is introduced. Further, a combination of nonlinear distribution of both binder concentration and ion release speed along the radial direction has yielded greater concavity in the wave front.

V. CONCLUSIONS AND FUTURE WORK

Our approach has several apparent advantages over others proposed, including ease of direct incorporation of structural complexity, and ease of addition of newly discovered mechanisms for ion release or binding. In a broader sense, we have provided a multilevel model for intracellular ionic transport, whose capabilities not generally available in other contemporary computational approaches.

In summary, there are three possible reasons to explain the concavity in the Ca²⁺ wave shape during the fertilization of *Xenopus* eggs: (1) the spherical shape of the domain; (2) the nonuniform distribution of Ca²⁺ diffusion speed; (3) the initial crescent distribution of triggering Ca²⁺ in the cortical regions due to the initial tangential development of IP₃ in that region. The last two make stronger contributions to the formation of the concave wave front. The first reason alone can only explain the wave shape in the late stage of wave propagation, but is unable to explain the consistency of the concavity from the very beginning. Also, nonuniformity in calcium ion release rate can change the wave front to a small extent, but cannot change the overall convexity of wave shape. With increased rate or volume of calcium release at one location, the probability of triggering a neighboring store is also higher, which could lead to a higher diffusion speed. However, this may not be enough to explain the experimental observation. The only possible way to achieve a reasonable correlation to experiments would be to assume escalating distribution of diffusion speed and tangential distribution of initial triggering Ca²⁺, per our simulations.

In addition, we provided an explanation for the observation [17] that diffusion speed is much higher at the wave initiation site and antipode: the change of diffusion speed may have resulted from misalignment of the observation plane.

Finally, it should be pointed out that Fontanilla and Nuccitelli [17] interpreted their images as representing a confocal "slice" through the center of the egg. However, the egg is nearly opaque [30,48], and what they imaged could be actually a cortical wave, and the slower velocity along a diameter can be expected simply from the spherical geometry. In order to test the hypothesis, more experiments should be conducted.

[1] M. J. Berridge, Nature (London) **395**, 645 (1993).

[2] M. J. Berridge, M. D. Bootman, and P. Lipp, Nature (London) **361**, 315 (1998).

[3] R. Deguchi and K. Osanai, Dev. Biol. **163**, 162 (1994).

[4] J. H. Horne and T. Meyer, Science **276**, 1690 (1997).

[5] A. McDougall, J. Shearer, and M. Whitaker, Biol. Cell **92**, 205 (2000).

[6] S. C. Tovey, P. De Smet, P. Lipp, D. Thomas, K. W. Young, L. Missiaen, H. De Smedt, J. B. Parys, M. J. Berridge, J. Thuring, A. Holmes, and M. D. Bootman, J. Cell. Sci. **114**, 3979 (2001).

[7] J. Marchant and I. Parker, EMBO J. **20**, 65 (2001).

[8] M. D. Bootman, E. Niggli, M. J. Berridge, and P. Lipp, J. Physiol. (London) **499**, 307 (1997).

[9] N. Callamaras, J. S. Marchant, X. P. Sun, and I. Parker, J. Physiol. (London) **509**, 81 (1998).

[10] M. D. Bootman, M. J. Berridge, and P. Lipp, Cell **91**, 367 (1997).

[11] M. R. Blaustein and V. A. Golovina, Trends Neurosci. **24**, 602 (2001).

[12] J. S. Marchant and C. W. Taylor, Curr. Biol. **7**, 510 (1997).

[13] M. D. Bootman, M. J. Berridge, and H. L. Roderick, Curr. Biol. **12**, R563 (2002).

[14] I. Bezprozvenny, *Organellar Ion Channels and Transporters*, (Rockefeller University Press, New York, 1996), p. 75.

[15] M. Tsukioka, M. Iino, and M. Endo, J. Physiol. (London) **475**, 369 (1994).

[16] J. W. Putney, Proc. Natl. Acad. Sci. U.S.A. **96**, 14669 (1999).

[17] R. A. Fontanilla and R. Nuccitelli, Biophys. J. **75**, 2079 (1998).

[18] C. W. Wang and A. M. Sastry, in *Encyclopedia of Biomaterials and Biomedical Engineering*, edited by G. E. Wenk and G. L. Bowlin (Marcel Dekker, New York, 2004), p. 355.

[19] J. Schaff, C. C. Fink, B. Slepchenko, J. H. Carson, and L. M. Loew, Biophys. J. **73**, 1135 (1997).

[20] C. C. Fink, B. Slepchenko, I. I. Moraru, J. Watras, J. C. Schaff, and L. M. Loew, Biophys. J. **79**, 163 (2000).

[21] Y. S. Choi, D. Resasco, J. Schaff, and B. Slepchenko, IMA J. Appl. Math. **62**, 207 (1999).

[22] S. Schuster, M. Marhl, and T. Hofer, Eur. J. Biochem. **269**, 1333 (2002).

[23] J. Keizer, G. D. Smith, S. Ponce-Dawson, and J. E. Pearson, Biophys. J. **75**, 595 (1998).

[24] A. E. Bugrim, A. M. Zhabotinsky, and I. R. Epstein, Biophys. J. **73**, 2897 (1997).

[25] M. Bar, M. Falcke, H. Levine, and L. S. Tsimring, Phys. Rev. Lett. **84**, 5664 (2000).

[26] M. Falcke, L. Tsimring, and H. Levine, Phys. Rev. E **62**, 2636 (2000).

[27] A. Gil, J. Segura, J. A. G. Pertusa, and B. Soria, Biophys. J. **78**, 13 (2000).

[28] J. Wagner, Y. X. Li, J. Pearson, and J. Keizer, Biophys. J. **75**, 2088 (1998).

[29] D. L. Gard, Microsc. Res. Tech. **44**, 388 (1999).

[30] A. E. Bugrim, R. Fontanilla, B. B. Eutenier, J. Keizer, and R. Nuccitelli, Biophys. J. **84**, 1580 (2003).

[31] J. Wagner, C. P. Fall, F. Hong, C. E. Sims, N. L. Allbritton, R. A. Fontanilla, I. I. Moraru, L. M. Loew, and R. Nuccitelli, Cell Calcium **35**, 433 (2004).

[32] J. Mishra and U. S. Bhalla, Biophys. J. **83**, 1298 (2002).

[33] M. D. Bootman and P. Lipp, Curr. Biol. **9**, R876 (1999).

[34] A. M. Sastry and C. M. Lastoskie, Proc. R. Soc. London, Ser. A **362**, 2851 (2004).

[35] B. E. Layton, A. M. Sastry, C. M. Lastoskie, M. A. Philbert, T. A. Miller, K. A. Sullivan, E. L. Feldman, and C.-W. Wang, BioTechniques **37**, 564 (2004).

[36] W. Shi, M. V. Inamdar, C. M. Lastoskie, and A. M. Sastry (unpublished).

[37] J. E. Estes, L. A. Selden, H. J. Kinosian, and L. C. Gershman, J. Muscle Res. Cell Motil. **13**, 272 (1992).

[38] H. Strzelecka-Golaszewska, G. Boguta, S. Zmorzynski, and J. Moraczewska, Eur. J. Biochem. **182**, 299 (1989).

[39] H. Strzelecka-Golaszewska, E. Prochniewicz, and W. Drabikowski, Eur. J. Biochem. **88**, 219 (1978).

[40] Y. B. Yi, A. M. Sastry, and M. A. Philbert (unpublished).

[41] B. Alberts, A. Johnson, J. Lewis, M. Raff, K. Roberts, and P. Walter, *Molecular Biology of the Cell*, 4th ed. (Garland Science, New York, 2002), p. 909.

[42] B. Ciapa and M. Whitaker, FEBS Lett. **195**, 347 (1985).

[43] K. Swann and M. Whitaker, J. Cell Biol. **103**, 2333 (1986).

[44] N. L. Allbritton, T. Meyer, and L. Stryer, Science **258**, 1812 (1992).

[45] G. De Young and J. Keizer, Proc. Natl. Acad. Sci. U.S.A. **89**, 9895 (1992).

[46] Y.-X. Li and J. Rinzel, J. Theor. Biol. **166**, 461 (1994).

[47] A. Atri, J. Amundson, D. Clapham, and J. Sneyd, Biophys. J. **65**, 1727 (1993).

[48] N. Callamaras and I. Parker, J. Gen. Physiol. **113**, 199 (1999).